


# Classical pilot-wave dynamics: The free particle


Cite as: Chaos **31**, 033136 (2021); <https://doi.org/10.1063/5.0039975>

Submitted: 08 December 2020 . Accepted: 18 February 2021 . Published Online: 12 March 2021

 Matthew Durey, and  John W. M. Bush

## COLLECTIONS

 This paper was selected as Featured

 This paper was selected as Scilight



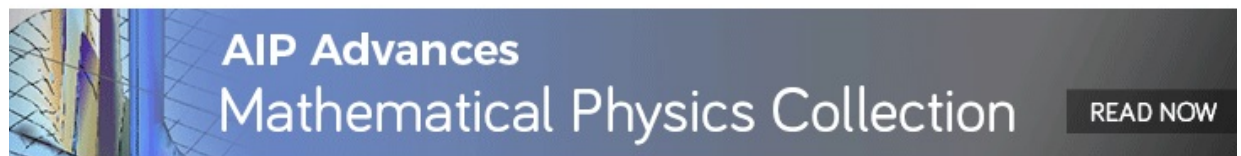
[View Online](#)



[Export Citation](#)



[CrossMark](#)



# Classical pilot-wave dynamics: The free particle



Cite as: Chaos 31, 033136 (2021); doi: 10.1063/5.0039975

Submitted: 8 December 2020 · Accepted: 18 February 2021 ·

Published Online: 12 March 2021



View Online



Export Citation



CrossMark

Matthew Durey<sup>a)</sup> and John W. M. Bush<sup>b)</sup>

## AFFILIATIONS

Department of Mathematics, Massachusetts Institute of Technology, Cambridge, Massachusetts 02139, USA

<sup>a)</sup> Author to whom correspondence should be addressed: [mdurey@mit.edu](mailto:mdurey@mit.edu)

<sup>b)</sup> [bush@math.mit.edu](mailto:bush@math.mit.edu)

## ABSTRACT

We present the results of a theoretical investigation into the dynamics of a vibrating particle propelled by its self-induced wave field. Inspired by the hydrodynamic pilot-wave system discovered by Yves Couder and Emmanuel Fort, the idealized pilot-wave system considered here consists of a particle guided by the slope of its quasi-monochromatic “pilot” wave, which encodes the history of the particle motion. We characterize this idealized pilot-wave system in terms of two dimensionless groups that prescribe the relative importance of particle inertia, drag and wave forcing. Prior work has delineated regimes in which self-propulsion of the free particle leads to steady or oscillatory rectilinear motion; it has further revealed parameter regimes in which the particle executes a stable circular orbit, confined by its pilot wave. We here report a number of new dynamical states in which the free particle executes self-induced wobbling and precessing orbital motion. We also explore the statistics of the chaotic regime arising when the time scale of the wave decay is long relative to that of particle motion and characterize the diffusive and rotational nature of the resultant particle dynamics. We thus present a detailed characterization of free-particle motion in this rich two-parameter family of dynamical systems.

Published under license by AIP Publishing. <https://doi.org/10.1063/5.0039975>

**The first macroscopic realization of a pilot-wave dynamics of the form proposed by de Broglie was discovered in 2005: an oil droplet may “walk” across the surface of a vertically vibrating fluid bath, propelled by its own wave field. This hydrodynamic pilot-wave system exhibits many features previously thought to be exclusive to the quantum realm, including orbital quantization and emergent wavelike statistics. We here present a theoretical investigation of an idealized pilot-wave system endowed with the dynamical features of the walking-droplet system critical to its quantum-like behavior. We pay particular attention to characterizing a new class of orbital states and the chaotic motion arising when the pilot wave is long lived. We thus provide a comprehensive characterization of the free-particle dynamics arising in this pilot-wave system.**

## I. INTRODUCTION

A millimetric, bouncing droplet may self-propel on the surface of a vertically vibrating fluid bath, guided by its accompanying Faraday wave field.<sup>1</sup> The decay time of the subcritical Faraday waves

increases with the magnitude of the vibrational forcing, thus increasing the longevity and propulsive influence of the waves generated along the droplet’s path. This decay time thus prescribes the extent of the droplet’s “path memory.”<sup>2</sup> In the long-path-memory limit, the quasi-monochromatic form of the guiding, or “pilot,” wave imposes a geometric constraint on the droplet dynamics that results in quantized dynamical states.<sup>3–6</sup> The pilot wave also leads to the emergence of quantum-like statistics, the origins of which may be characterized in terms of three distinct paradigms:<sup>6,7</sup> (i) chaotic switching between weakly unstable quantized periodic dynamical states;<sup>4,8–10</sup> (ii) in-line speed oscillations over the length scale of the pilot wave;<sup>11</sup> and (iii) asymptotic diffusion arising from the droplet’s random-walk-like motion across its pilot-wave field.<sup>7,12–14</sup>

While the walking-droplet system is the first classical realization of a pilot-wave dynamics of the form proposed by de Broglie,<sup>15,16</sup> its limitations as a quantum analog prompted Bush<sup>5</sup> to propose the theoretical exploration of a new class of pilot-wave systems. These idealized systems retain the salient features of the hydrodynamic system while side-stepping some of its complexity; moreover, they can be probed beyond the experimental regime of walking droplets, yielding new insight into the potential for quantum-like

behavior in classical systems. Within the pilot-wave framework considered here,<sup>5</sup> the dynamics of a free particle may be characterized in terms of just two dimensionless parameters, allowing for a relatively straightforward exploration of parameter space.

As the generalized pilot-wave system considered here is rooted in the stroboscopic model of pilot-wave hydrodynamics developed by Oza *et al.*,<sup>17</sup> it has certain features in common with the walking-droplet system, including a steady rectilinear self-propelling state<sup>1,2,7,17–21</sup> and in-line speed oscillations.<sup>7,13,22,23</sup> The generalized pilot-wave system also has features that have been identified in various theoretical models of the hydrodynamic system but have not been observed in the laboratory. Of particular interest to the present study are *spin* states,<sup>24–26</sup> in which a particle executes a circular orbit by virtue of the confining influence of its pilot-wave field, and the erratic particle motion arising in the long-path-memory limit.<sup>7,13,14,27–29</sup>

The generalized pilot-wave system also gives rise to dynamical features that have been observed in neither the walking-droplet system nor theoretical models thereof. For example, when a particle is confined by an oscillatory potential (of the form of a Bessel function), it may switch intermittently between different orbital states, resulting in a dynamically unstable, statistically steady state. The long-time dynamics thus give rise to a wavelike statistical form,<sup>30</sup> consistent with the first paradigm for the emergence of quantum-like statistics in the walking-droplet system. When the interaction of particle pairs was considered in this generalized framework, a variety of periodic and chaotic bound states were shown to arise,<sup>31</sup> demonstrating the richness of this new class of dynamical system.

Certain features of a free particle in the generalized pilot-wave system evoke classical models of quantum systems. For example, spin states are similar in form to the classical model of the electron.<sup>32</sup> The in-line oscillations and *jittering* motion<sup>7</sup> of the free particle evoke the so-called *Zitterbewegung*, the trembling of a quantum particle over the Compton time scale, a feature of early models of quantum dynamics.<sup>33,34</sup> Of particular interest here is the statistical manifestation of structured random walks arising in the long-path-memory limit.<sup>7,13,14,27–29</sup> Such random walks result in asymptotic particle diffusion, giving rise to a quantum-like statistical form<sup>28,29</sup> and a physical picture reminiscent of Nelson's stochastic mechanics,<sup>35</sup> in which quantum dynamics is imagined as a diffusive process with diffusivity  $\mathcal{D} = \hbar/(2m)$ , where  $\hbar$  is the reduced Planck constant and  $m$  the particle mass.<sup>6</sup>

Hubert *et al.*<sup>13</sup> recently examined a new form of erratic pilot-wave dynamics arising in their theoretical model of the walking-droplet system. The droplet motion is characterized in terms of a run-and-tumble dynamics,<sup>36,37</sup> for which the resulting chaos is of the Shil'nikov type, as arises when a homoclinic cycle interacts with a subcritical Hopf bifurcation.<sup>38,39</sup> In the context of pilot-wave dynamics, the subcritical Hopf bifurcation corresponds to the instability of the steady rectilinear self-propelling state,<sup>7,13,14</sup> the homoclinic cycle to the transition of the particle between neighboring peaks of its pilot wave.<sup>14</sup> The authors further show that the erratic particle motion exhibits asymptotic diffusion, with the corresponding diffusion coefficient decreasing with increasing path memory. We will examine here similar run-and-tumble dynamics in the context of our generalized pilot-wave framework, characterizing the relative influence of particle inertia, drag and wave forcing on the particle motion.

We here provide a relatively comprehensive description of the free-particle dynamics in our generalized pilot-wave system. In Sec. II, we formulate the idealized pilot-wave system of interest and devise a new numerical method for efficiently evolving the pilot-wave system (Sec. II A). Using this numerical scheme, we identify and delineate regimes in which stable rectilinear and orbital states arise (Sec. II B). In Sec. III, we characterize new wobbling and precessing orbital states that arise just beyond the stability boundary of the spin states. In Sec. IV, we explore the regime in which steady self-propulsion is unstable, elucidating the rotational and diffusive nature of the particle's chaotic motion. Finally, in Sec. V, we discuss our results in the context of prior studies of the hydrodynamic pilot-wave system and recent realist models of quantum dynamics.

## II. CLASSICAL PILOT-WAVE DYNAMICS

We consider an idealized dynamical system in which a vibrating particle is propelled by the local slope of its guiding quasi-monochromatic wave field and resisted by drag. Specifically, we consider the evolution of a particle of mass  $m$  with position  $\mathbf{x}_p(t)$  at time  $t$ , where the particle vibrates with period  $T$ , generating axisymmetric standing waves about the particle's instantaneous position. Time-averaging the system over one vibration period<sup>19</sup> yields a trajectory equation of the form

$$m\ddot{\mathbf{x}}_p + D\dot{\mathbf{x}}_p = -F\nabla h(\mathbf{x}_p, t), \quad (1a)$$

where  $D$  is a linear drag coefficient,  $F$  is the time-averaged force exerted by the particle-wave interaction,  $h(\mathbf{x}, t)$  is the time-averaged pilot wave, and dots denote differentiation with respect to time. We posit that the pilot wave,  $h(\mathbf{x}, t)$ , may be expressed as the superposition of quasi-monochromatic, axisymmetric waves generated along the particle path. The waves decay exponentially in time over a time scale  $\tau$  that prescribes the longevity of the particle's path-memory. We thus consider a pilot-wave form

$$h(\mathbf{x}, t) = \frac{A}{T} \int_{-\infty}^t J_0(k|\mathbf{x} - \mathbf{x}_p(s)|) e^{-(t-s)/\tau} ds, \quad (1b)$$

where  $A$  is the amplitude of the wave generated at each instant in time,  $\lambda = 2\pi/k$  is the wavelength of the pilot wave, and  $J_0$  is the Bessel function of the first kind with order zero.<sup>17</sup>

The stationary state, characterized by  $\mathbf{x}_p = \text{constant}$  and  $h(\mathbf{x}) = (A\tau/T)J_0(k|\mathbf{x} - \mathbf{x}_p|)$ , destabilizes when the memory time,  $\tau$ , exceeds the critical threshold<sup>7,17</sup>

$$\tau_0 = \sqrt{\frac{2DT}{FAk^2}}, \quad (2)$$

beyond which sustained particle self-propulsion ensues. To characterize the free-particle dynamics arising beyond this critical threshold ( $\tau > \tau_0$ ), we non-dimensionalize the pilot-wave system (1) by scaling lengths with the inverse pilot-wavenumber,  $\mathbf{x} \sim k^{-1}$ , time with the memory time at the onset of self-propulsion,  $t \sim \tau_0$ , and the pilot-wave amplitude by that at the instability threshold,  $h \sim A\tau_0/T$ . These rescalings result in the dimensionless pilot-wave system

$$\kappa_0 \ddot{\mathbf{x}}_p + \dot{\mathbf{x}}_p = -2\nabla h(\mathbf{x}_p, t), \quad (3a)$$

$$h(\mathbf{x}, t) = \int_{-\infty}^t J_0(|\mathbf{x} - \mathbf{x}_p(s)|) e^{-\mu(t-s)} ds, \quad (3b)$$

where  $\kappa_0 = m/D\tau_0$  and  $\mu = \tau_0/\tau$  are dimensionless parameters characterizing the particle inertia<sup>5,26</sup> and wave damping,<sup>7,14</sup> respectively.

As follows from (3b), the time scale over which the wave force,  $-2\nabla h(\mathbf{x}_p, t)$ , is influenced by the particle path is  $1/\mu$ , and diverges in the long-path-memory limit,  $\mu \rightarrow 0$ . To characterize the extent of the path memory, we define  $\Gamma = 1 - \mu$ , where  $\Gamma = 0$  at the onset of particle self-propulsion and  $\Gamma = 1$  is the limit at which the wave damping vanishes. The parameter  $\Gamma$  may thus be seen to be equivalent to the normalized vibrational forcing in the related hydrodynamic system, with  $\Gamma = 1$  corresponding to the Faraday threshold.<sup>5,26</sup> We henceforth refer to the pilot-wave system (3) as the *generalized* stroboscopic model. By varying the system parameters, we may explore a parametric generalization of Oza *et al.*'s<sup>17</sup> stroboscopic model of pilot-wave hydrodynamics.<sup>5,26</sup> As this model is rooted in the walking-droplet system, we anticipate a number of dynamical commonalities, which we summarize below. However, by exploring parameter regimes inaccessible in the walking-droplet system, we identify new stable orbital states arising in the generalized stroboscopic model.

### A. Numerical method

In order to explore the dynamics of the generalized stroboscopic model, we here develop a new numerical framework for evolving the pilot-wave system (3). We first recall that the pilot-wave system (3) exhibits translational invariance, a property that we exploit by expressing the wave field in the frame of reference moving with the particle.<sup>7,13</sup> We then consider the basis decomposition<sup>13</sup>

$$h(\mathbf{x}, t) = a_0(t) J_0(|\mathbf{x} - \mathbf{x}_p(t)|) + \sum_{n=1}^{\infty} 2\text{Re}[a_n(t) \Phi_n(\mathbf{x} - \mathbf{x}_p(t))], \quad (4)$$

where the complex basis functions  $\Phi_n(\mathbf{x}) = J_n(r) e^{in\theta}$  are defined in terms of the imaginary unit,  $i$ , and the polar coordinates  $(r, \theta)$ , which satisfy  $\mathbf{x} = r(\cos \theta, \sin \theta)$ .

It remains to determine evolution equations for the complex wave coefficients,  $a_n(t)$ . As detailed in Appendix A, it follows from Eq. (3b) that the wave coefficients evolve according to

$$\dot{a}_0 - \text{Re}[\dot{z}_p a_1] + \mu a_0 = 1, \quad (5a)$$

$$\dot{a}_n - \frac{1}{2} [\dot{z}_p a_{n+1} - \dot{z}_p^* a_{n-1}] + \mu a_n = 0, \quad \forall n \geq 1, \quad (5b)$$

where  $z_p(t) = x_p(t) + iy_p(t)$  is the particle position,  $\mathbf{x}_p = (x_p, y_p)$ , represented in the complex plane and  $*$  denotes complex conjugation. In the complex form, the particle evolution equation (3a) becomes

$$\kappa_0 \ddot{z}_p + \dot{z}_p + 2a_1^* = 0. \quad (5c)$$

We numerically evolve the complex representation of the pilot-wave system (5) using a fourth-order Runge-Kutta method with appropriate truncation of the wave coefficients,  $a_n$ , details of which are provided in Appendix A.

### B. Regime diagram

We proceed by characterizing the dynamics of the generalized stroboscopic model in the entirety of the  $(\kappa_0, \Gamma)$ -plane (see Fig. 1). Beyond the onset of instability of the stationary state ( $\Gamma > 0$ ), the particle executes rectilinear motion at a constant speed<sup>7,17</sup>

$$u_0 = \frac{1}{\sqrt{2}} \left( 4 - \mu^2 - \mu \sqrt{\mu^2 + 8} \right)^{1/2} \quad (6)$$

in an arbitrary direction. For small  $\Gamma$ , the response of the particle when perturbed from steady rectilinear propulsion is characterized by overdamped oscillations.<sup>17</sup> As  $\Gamma$  is increased, the perturbations become underdamped, exhibiting speed modulations over a length scale comparable to the wavelength of the pilot wave.<sup>7</sup> For  $\Gamma > \Gamma_c$ , steady rectilinear propulsion destabilizes via a subcritical Hopf bifurcation<sup>7</sup> and erratic particle motion ensues.<sup>13</sup> The particle exhibits growing speed oscillations until it reverses direction and is temporally trapped by its accompanying wave form,<sup>13</sup> a dynamics we further detail in Sec. IV.

Spin states<sup>24-26</sup> may also arise in the generalized stroboscopic model. Such states are characterized in terms of their orbital radius,  $r_0$ , and angular frequency,  $\omega_0$ , which satisfy the following pair of algebraic equations:<sup>10,24,26</sup>

$$-\kappa_0 r_0 \omega_0^2 = 2 \int_0^{\infty} J_1 \left( 2r_0 \sin \frac{\omega_0 s}{2} \right) \sin \frac{\omega_0 s}{2} e^{-\mu s} ds, \quad (7a)$$

$$r_0 \omega_0 = 2 \int_0^{\infty} J_1 \left( 2r_0 \sin \frac{\omega_0 s}{2} \right) \cos \frac{\omega_0 s}{2} e^{-\mu s} ds. \quad (7b)$$

As delineated by Oza *et al.*,<sup>26</sup> spin states are stable only for  $\kappa_0 < 0.183$  (see Fig. 1). The corresponding orbital radius,  $r_0$ , is well-approximated by the first zero of the Bessel function,  $J_0(\kappa r_0) = 0$ , yielding  $r_0/\lambda \simeq 0.38$ , while the orbital speed,  $r_0 \omega_0$ , is generally comparable to that of the steady rectilinear propulsion speed,  $u_0$ .<sup>26</sup>

Just beyond the boundary at which spin states destabilize, we identify a small region of parameter space in which a new class of dynamical states emerges, taking the form of stable wobbling and precessing orbital trajectories (see Sec. III). We note that these relatively complex orbital motions all coexist with stable rectilinear propulsion and may thus only be found with specific initialization of the pilot-wave system. Moreover, there is a minute portion of parameter space (depicted by the white region in Fig. 1) in which stable wobbling, precessing, and rectilinear propulsion all coexist, highlighting the richness of this generalized stroboscopic pilot-wave system.

As the pilot wave is central to the propulsion of the particle, it is informative to compare its form for the different dynamical states. As presented in Fig. 2(a), the pilot wave accompanying steady rectilinear propulsion has a horseshoe-like form ahead of the particle, with an interference pattern apparent in the particle's wake, reminiscent of that arising in the walking-droplet system.<sup>1,2,17,18,20,21,40</sup> As is evident in Fig. 2(b), the wave field accompanying orbital motion is markedly different in form to that of rectilinear propulsion and serves to confine the particle to its circular trajectory.<sup>26</sup> The evolution of the pilot wave accompanying wobbling, precessing, and erratic states is presented in the [supplementary material](#).

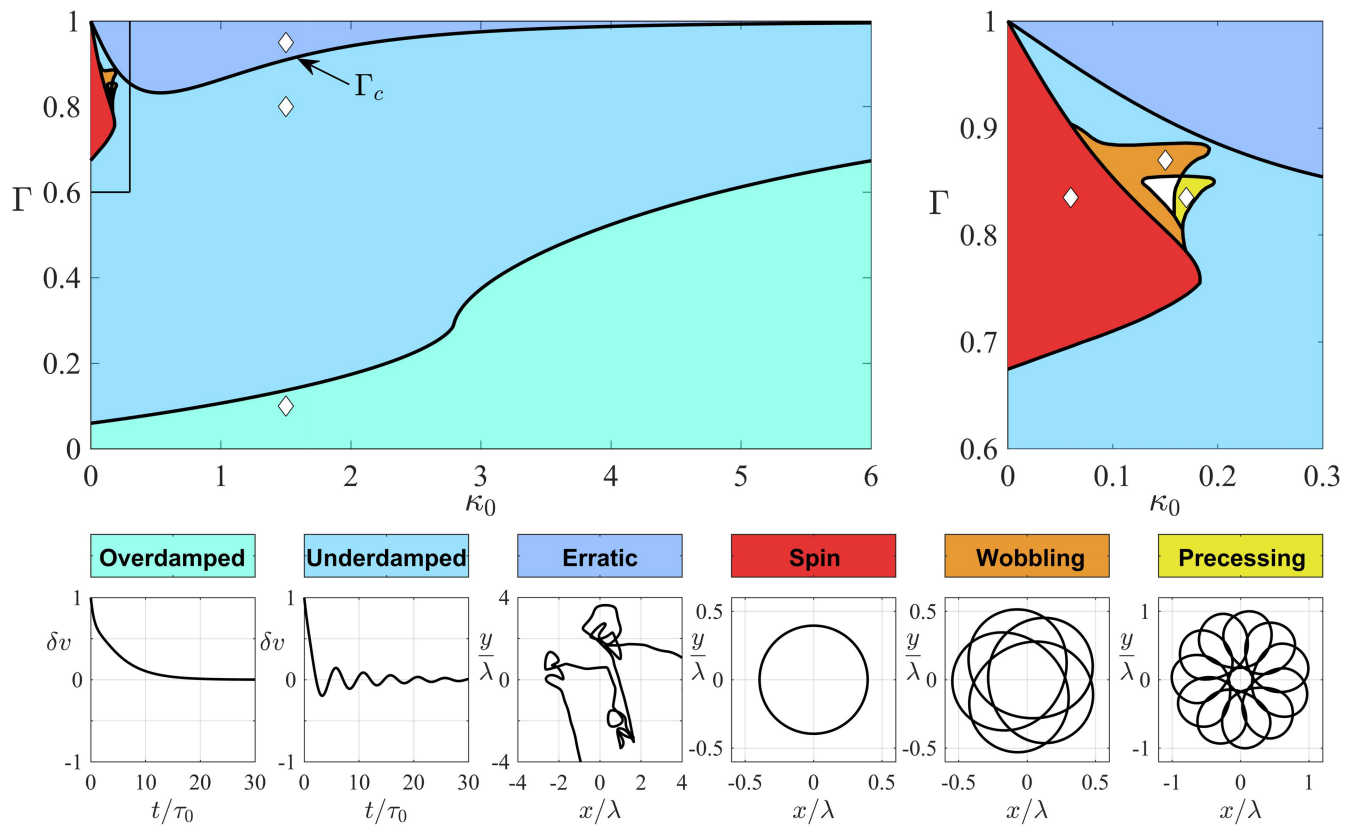


**FIG. 1.** Regime diagram delineating the emergent dynamical states, as classified in the legend. As  $\Gamma$  is increased, perturbations from the steady self-propelling state transition from overdamped to underdamped oscillations. In the long-path-memory limit ( $\Gamma > \Gamma_c$ ), the particle destabilizes into erratic motion. For  $\kappa_0 < 0.183$ , stable spin states may arise. Spin states may destabilize into stable wobbling and precessing trajectories, both of which exist within the white region. All such stable orbital states coexist with stable rectilinear self-propelling states. White diamonds define the parameter values of the trajectories presented in the legend. The small speed perturbation,  $\delta v(t)$ , presented in the legend is normalized such that  $\delta v(0) = 1$ .

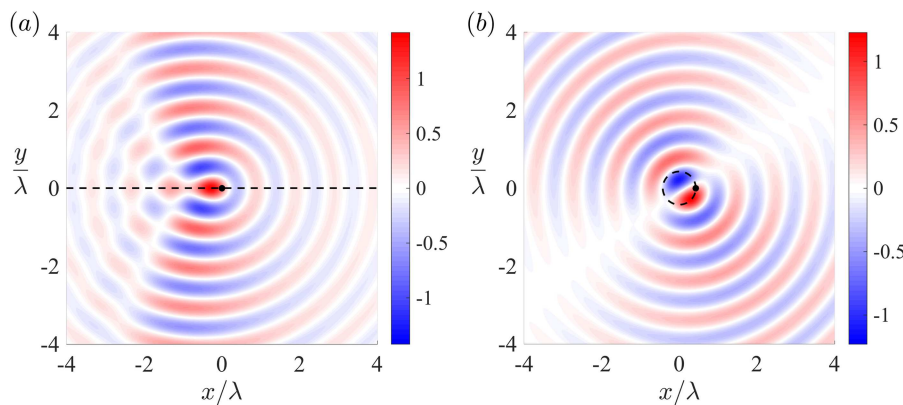


**FIG. 2.** The form of the pilot wave,  $h(\mathbf{x}, t)$ , for two coexisting stable states arising at  $\Gamma = 0.75$  and  $\kappa_0 = 0.15$ . (a) Steady rectilinear particle population at speed  $u_0$  in the positive  $x$ -direction. (b) A spin state, characterized by counterclockwise circular motion. In both panels, dashed lines denote the particle path and dots denote the instantaneous particle position. The amplitude of the pilot wave,  $h(\mathbf{x}, t)$ , is normalized by  $A\tau_0/T$ .

### III. WOBBLING AND PRECESSING ORBITS

We proceed by characterizing the form of the wobbling and precessing orbital states arising near the boundary of the parameter regime containing stable spin states. We first observe that, as evident in Fig. 1, wobbling and precessing trajectories only arise for  $0.79 < \Gamma < 0.91$ . While a large wave force is required to trap the particle on an orbital path, these orbital states all destabilize at sufficiently high  $\Gamma$ . Moreover, wobbling and precessing states arise only for  $\kappa_0 < 0.2$ : as inertial effects are increased, the particle's tendency for rectilinear propulsion is enhanced, resulting in the destabilization of orbital motion.

In order to characterize wobbling and precessing orbital states, we first translate the coordinate system so that the origin is the average position of the particle over its entire trajectory. We then define the particle's instantaneous radial displacement,  $r_p(t) = |\mathbf{x}_p(t)|$ , and orbital period,  $P$ , which satisfy  $r_p(t) = r_p(t + P)$  for all  $t$ . Furthermore, we denote the moving average of the particle position over one orbital period by the orbital center,  $\mathbf{x}_c(t)$ , defined as<sup>9,10</sup>

$$\mathbf{x}_c(t) = \frac{1}{P} \int_t^{t+P} \mathbf{x}_p(s) ds.$$

The relationship between the orbital center,  $\mathbf{x}_c(t)$ , and the orbital trajectory,  $\mathbf{x}_p(t)$ , for wobbling and precessing states is illustrated in Fig. 3. The orbital center of a wobbling orbit remains close to the origin, tracing a trajectory similar in form to the particle path. In contrast, the orbital center of a precessing trajectory resembles a hypocycloid, with characteristic cusps denoting the centers of the successive loops of the particle trajectory.

We also characterize the orbital trajectory in terms of the instantaneous radius of curvature,  $R(t)$ , which necessarily decreases in magnitude for tighter loops. The radius of curvature is defined as

$$R = \frac{|\dot{\mathbf{x}}_p|^3}{|\dot{\mathbf{x}}_p \wedge \ddot{\mathbf{x}}_p|},$$

where  $\wedge$  denotes the vector product. Notably, for a circular orbit of radius  $r_0$ , the orbital radius, radial displacement and radius of curvature are all equal ( $r_0 = r_p = R$ ) and the orbital center is the origin ( $\mathbf{x}_c = \mathbf{0}$ ).

As evident in Fig. 4, the radial displacement and radius of curvature of wobbling orbits (red curves) remain close to the orbital radius,  $r_0$ , departing to a greater extent as  $\kappa_0$  is increased (with  $\Gamma$

fixed). This behavior is suggestive of a supercritical Hopf bifurcation as  $\kappa_0$  is increased beyond the instability threshold of spin states. The particle speed,  $v(t) = |\dot{\mathbf{x}}_p(t)|$ , varies along the trajectory, achieving a maximum value when the radial displacement,  $r_p$ , is greatest (see Fig. 3). Moreover, the average orbital speed is typically comparable to the steady rectilinear propulsion speed,  $u_0$ , defined in Eq. (6). For precessing orbits (blue curves in Fig. 4), the particle trajectory exhibits relatively large variations in radial displacement,  $r_p(t)$ , and radius of curvature,  $R(t)$ . Although the bounds of  $r_p$  increase with  $\kappa_0$ , we observe that the bounds of  $R$  remain approximately constant; indeed, the average value of  $R$  remains close to half the wavelength of the pilot wave. We observe that the speed variations along precessing trajectories are much greater than those along wobbling orbits; however, as on wobbling orbits, the maximum particle speed arises when the particle is at the extremities of its orbit (see Fig. 3).

We proceed by considering the angular displacement (in degrees),  $\delta\theta$ , of the particle over one orbital period,  $P$ ,

$$\delta\theta = \arccos \frac{\mathbf{x}_p(t) \cdot \mathbf{x}_p(t+P)}{r_p^2(t)}. \tag{8}$$

We note that we have simplified the definition of  $\delta\theta$  using the periodicity of  $r_p(t)$ . As presented in Fig. 4, the period,  $P$ , and angular displacement,  $\delta\theta$ , both vary monotonically with increasing  $\kappa_0$ , the period increasing and the angular displacement decreasing. In general, the angular displacement is not a divisor of  $360^\circ$ , resulting in the azimuthal drift of the orbital loops. We note the possibility of an unstable branch connecting the wobbling and precessing orbital states, as would provide a mechanism for the hysteresis observed as  $\kappa_0$  is varied. Further investigation into this possibility will be left for future consideration.

We define the instantaneous angular speed,  $\omega(t)$ , of the particle as the product of its speed and the local curvature of the trajectory,  $\omega = v/R$ . We note that the angular speed is largest when the particle executes a sharp change in direction, vanishes for rectilinear particle motion, and equals the orbital angular frequency,  $\omega_0$ , for spin states. In Fig. 5, we present the evolution and bounds of the normalized angular speed,  $\omega/\omega_0$ , for the orbital states. We observe that the instantaneous angular speed for wobbling states oscillates about  $\omega_0$ , resulting in a mean comparable to that of spin states. In contrast, the angular speed for precessing trajectories exhibits far greater variations and the resultant mean is appreciably less than

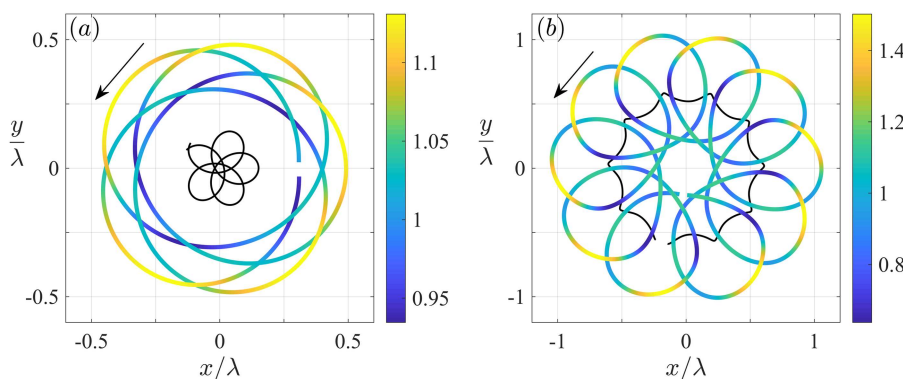


**FIG. 3.** Orbital trajectories arising at  $\Gamma = 0.85$ . (a) Wobbling trajectory at  $\kappa_0 = 0.13$ . (b) Precessing loops at  $\kappa_0 = 0.18$ . In both panels, the trajectory is color-coded by the particle speed normalized by that of a free particle,  $v/u_0$ . The orbital center,  $\mathbf{x}_c(t)$ , is superimposed (black curve), and the arrow denotes the direction of particle motion.

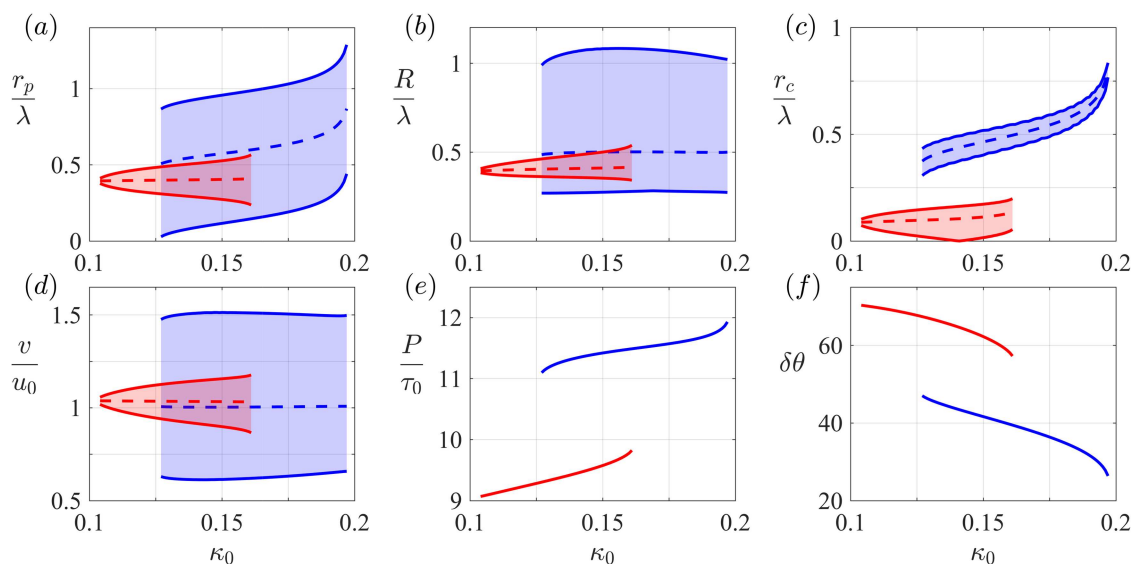


**FIG. 4.** Wobbling and precessing orbital states arising at  $\Gamma = 0.85$ , with  $\kappa_0$  in the range 0.104–0.197. (a) The average (dashed curves) and the upper and lower bounds (solid curves) of the particle’s radial displacement,  $r_p$ , for wobbling (red) and precessing (blue) trajectories. (b) The associated radius of curvature,  $R$ . (c) The radial displacement of the orbital center,  $r_c = |\mathbf{x}_c|$ . (d) The normalized particle speed,  $v/u_0$ . (e) The orbital period,  $P$ . (f) The orbital angular displacement (in degrees),  $\delta\theta$ , as defined in Eq. (8).

$\omega_0$  [see Fig. 5(c)]. The difference in the mean angular speed may be attributed to the difference between the average radius of curvature for wobbling and precessing trajectories, as quantified in Fig. 4(b). However, for both wobbling and precessing trajectories, the maximum angular speed arises when the radial displacement of the particle is greatest, coinciding with maxima in both particle speed and curvature.

**IV. ERRATIC DYNAMICS**

We proceed by exploring the particle dynamics arising in the regime where steady rectilinear propulsion is unstable ( $\Gamma > \Gamma_c$ ).

We characterize the dynamics in this regime in terms of two distinct phases, laminar and erratic<sup>13</sup> [see Fig. 6(a)], as related to those arising in the canonical run-and-tumble dynamics.<sup>36,37</sup> In the laminar (or “run”) phase, the particle motion is rectilinear but accompanied by growing speed oscillations [see Fig. 6(b)]. Eventually, the speed oscillations become so large that the particle reverses direction, triggering a switch from laminar to erratic motion. The erratic (or “tumble”) phase is characterized by unpredictable changes in particle direction associated with the particle navigating its complex wave field. When the particle eventually escapes the confining influence of its wave field, it resumes unsteady rectilinear motion.

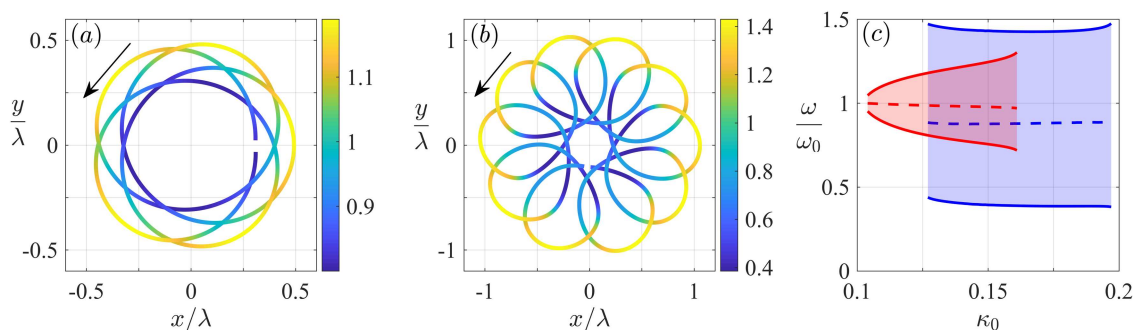


**FIG. 5.** The angular speed of wobbling and precessing orbital states arising at  $\Gamma = 0.85$ . (a) The instantaneous normalized angular speed,  $\omega/\omega_0$ , for a wobbling trajectory arising at  $\kappa_0 = 0.13$ . The arrow denotes the direction of particle motion. (b) The instantaneous normalized angular speed for a precessing trajectory arising at  $\kappa_0 = 0.18$ . (c) The mean (dashed curves) and bounds (solid curves) of the normalized angular speed for wobbling (red) and precessing (blue) trajectories arising for  $\kappa_0$  in the range 0.104–0.197.

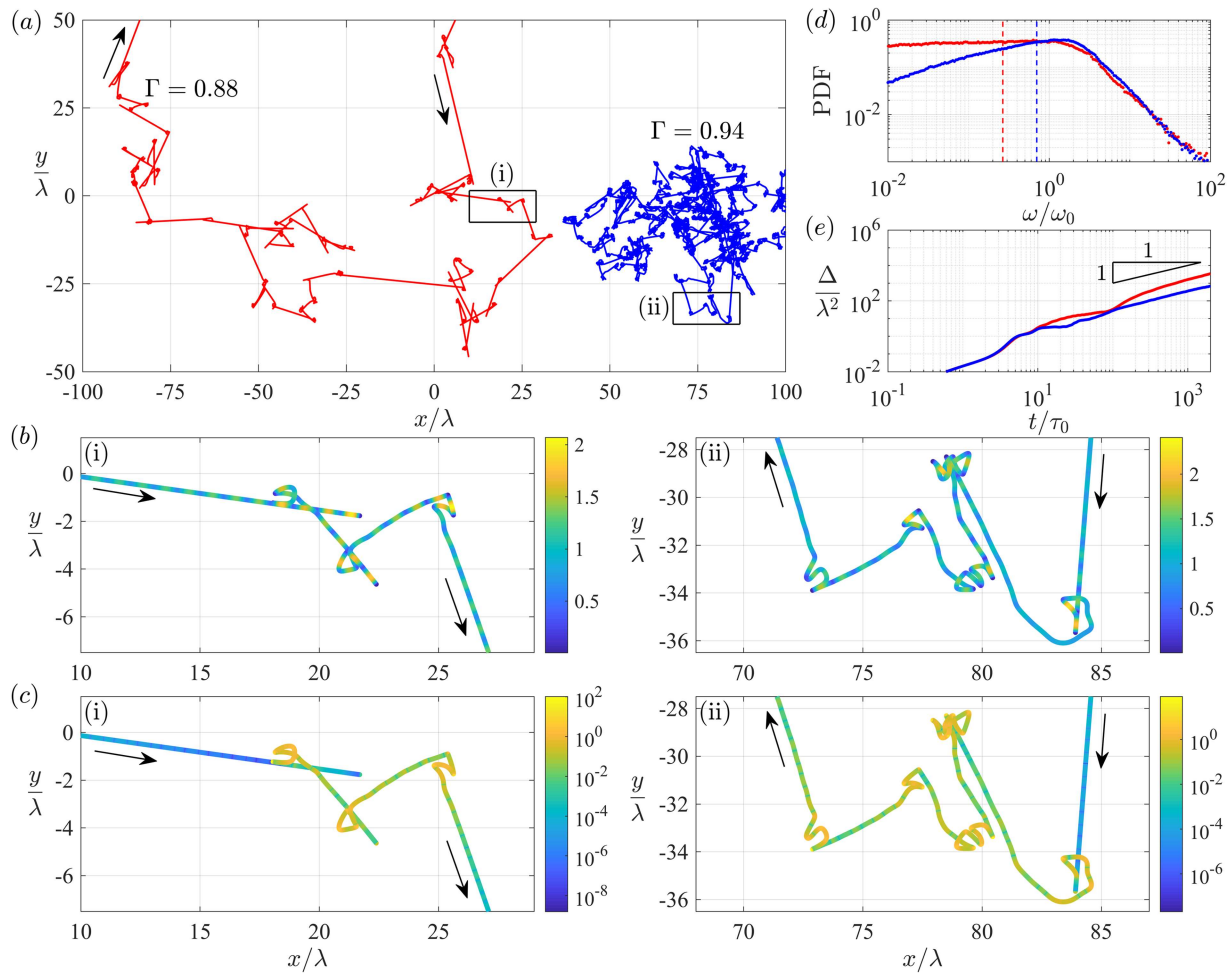


**FIG. 6.** Erratic pilot-wave dynamics arising at  $\kappa_0 = 1$ , with  $\Gamma = 0.88$  (red) and  $\Gamma = 0.94$  (blue). (a) Sample particle trajectories. (b) and (c) Panels (i) and (ii) present subtrajectories from (a), color-coded by (b) the instantaneous normalized speed,  $v/u_0$ , and (c) the instantaneous normalized angular speed,  $\omega/\omega_0$ . Arrows denote the direction of particle motion. (d) Corresponding probability density function (PDF, dots) of the normalized angular speed,  $\omega/\omega_0$ , computed over a single simulation of duration  $50\,000\tau_0$  [see Eq. (2)]. The mean value of  $\omega/\omega_0$  is represented by the dashed line for each value of  $\Gamma$ . (e) Corresponding evolution of the mean-squared displacement,  $\Delta(t)$ , averaged over  $N_0 = 1000$  similarly prepared systems. The long-time behavior,  $\Delta(t) \sim 2Dt$  as  $t \rightarrow \infty$ , is indicative of asymptotic diffusion, where  $\mathcal{D}$  is the diffusion coefficient.

We proceed by considering the influence of both the path memory and particle inertia (characterized by  $\Gamma$  and  $\kappa_0$ , respectively) on both the asymptotic diffusivity and rotational nature [see Fig. 6(c)] of this chaotic dynamics in the context of the generalized stroboscopic model.

As the path memory increases, the more erratic nature of the particle trajectory results in an overall increase in the average angular speed [see Fig. 6(d)]. In order to characterize the particle diffusivity, we consider a Monte-Carlo-like series of numerical simulations of an ensemble of  $N_0$  similarly prepared systems. We then characterize the diffusivity in terms of the mean-squared displacement,  $\Delta(t) = N_0^{-1} \sum_{n=1}^{N_0} |\mathbf{x}_n(t) - \mathbf{x}_n(0)|^2$ , where  $\mathbf{x}_n(t)$  is the particle trajectory for the  $n^{\text{th}}$  realization. The asymptotic diffusion coefficient,  $\mathcal{D}$ ,

is defined so as to satisfy  $\Delta(t) \sim 2Dt$  as  $t \rightarrow \infty$ . In the long path-memory limit, the prevalence of the erratic tumble phase decreases the corresponding diffusion coefficient,<sup>13</sup> as evident in Fig. 6(e). The particle typically thus explores the plane less efficiently when the path memory is increased.

For different values of the inertial coefficient,  $\kappa_0$ , we observe similar trends in the diffusion coefficient and mean angular speed as  $\Gamma$  is increased (see Fig. 7). Specifically, the diffusion coefficient,  $\mathcal{D}$ , is maximal at the instability threshold of steady rectilinear propulsion ( $\Gamma \gtrsim \Gamma_c$ ) and decreases with increasing  $\Gamma$ ,<sup>13</sup> while the mean angular speed is smallest at the instability threshold and increases with increasing  $\Gamma$ . We note that the largest values of the diffusion coefficient and the smallest values of the mean angular speed are achieved



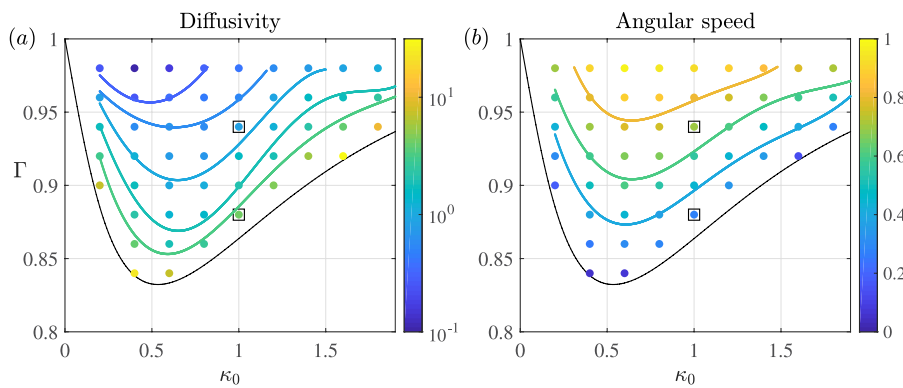


**FIG. 7.** Characterization of the erratic pilot-wave dynamics arising for  $\Gamma > \Gamma_c$  (above the black curve). (a) The normalized asymptotic diffusion coefficient,  $\mathcal{D}/\lambda u_0$ , computed by averaging over  $N_0 = 1000$  similarly prepared systems. (b) The normalized mean angular speed,  $\omega/\omega_0$ , averaged over a single simulation of duration  $50\,000\tau_0$ . In both panels, the dots are simulation results and the curves are visual guides, representative of contours. The squares correspond to the parameter values shown in Fig. 6.

for similar values of  $\kappa_0$ . Specifically, these extrema are achieved near the minimizer of the instability curve,  $\Gamma_c(\kappa_0)$ , corresponding to  $\kappa_0 \approx 0.5$ .

## V. DISCUSSION

We have explored the dynamics of the generalized stroboscopic pilot-wave system,<sup>5,26</sup> in which a vibrating particle is guided by its self-generated wave field. A new numerical framework has allowed for an efficient exploration thereof. Our investigation has furthered the characterization of the free particle, delineating regimes in which steady rectilinear propulsion and orbital motion are stable dynamical states. We have identified regimes in which new stable wobbling and precessing orbits arise. We have demonstrated that these stable orbital states coexist with stable rectilinear propulsion and may only be accessed via specific initializations of the pilot-wave system. In the precessing state, the particle executes periodic loops superimposed on a hypocycloid-like trajectory. If a spin state is taken to be a classical analog of the electron,<sup>32</sup> then these precessing orbits would correspond to an orbiting electron. This analog electron would then possess two distinct forms of angular momentum that one might refer to as intrinsic and orbital.

We have also characterized the diffusive and rotational nature of the particle's chaotic motion, as arises when  $\Gamma > \Gamma_c$ .<sup>13</sup> In the chaotic regime, the particle motion exhibits successive laminar and erratic phases. The particle motion becomes increasingly erratic as the path memory is increased, resulting in an increase of the average angular speed and a corresponding decrease of the particle's asymptotic diffusion coefficient.<sup>13</sup> These trends appear to be independent of the inertial coefficient,  $\kappa_0$ , which serves only to set the instability threshold,  $\Gamma_c(\kappa_0)$ , of steady rectilinear self-propulsion.

As a caveat, we note that although our exploration of the  $(\kappa_0, \Gamma)$  parameter space (see Fig. 1) is relatively comprehensive, we cannot rule out the possibility that more exotic dynamical states might be found from initializations of the pilot-wave system other than those considered here. Similarly, stable dynamical states might arise within small pockets of parameter space when  $\Gamma > \Gamma_c$ , despite the system's propensity for chaotic particle motion at long path-memory.

Our study has characterized new orbital states, specifically wobbling and precessing spin states, for the free particle. While similar orbital motions (spin, wobbling, and precessing states) also arise

in the hydrodynamic system,<sup>9,10</sup> they are only stable when the droplet is subjected to an applied force. It would thus be illuminating to explore further the influence of applied forces on the particle motion in our generalized pilot-wave framework. The aim of such investigations would be to extend existing numerical studies of the emergent orbital and chaotic dynamics in the presence of Coriolis<sup>3,9,10,24</sup> or central<sup>4,21,41,42</sup> forces to parameter regimes beyond those accessible with the hydrodynamic pilot-wave system. Of particular interest would be the delineation of regimes in which multiple stable attractors coexist, as has already been shown to be the case for particle motion confined to a line<sup>7,14,23,29</sup> and for orbital dynamics.<sup>3,9,24</sup> It would also be intriguing to consider the symmetry-breaking effect of a Coriolis force on the particle's rotational motion in the chaotic regime and appeal to the analogy between the Coriolis and Lorentz forces in order to characterize the emergent magnetization.

Finally, it is interesting to connect our work with recent pilot-wave models of quantum dynamics inspired by the walking-droplet system.<sup>43–46</sup> In the hydrodynamic quantum field theory of Dagan and Bush,<sup>43</sup> a particle is propelled by the slope of a pilot wave evolving according to the forced Klein–Gordon equation. As the form of this model of quantum dynamics is rooted in the walking-droplet system, we anticipate a number of dynamical commonalities. Indeed, the simulations of Dagan and Bush of one-dimensional particle motion revealed speed oscillations with the length scale of the pilot wave<sup>7,13,22,23</sup> and an irregular *jittering* motion.<sup>7,14</sup> An exploration of this hydrodynamic quantum field theory in two spatial dimensions<sup>44</sup> would allow one to determine whether analogous self-induced orbital motion and stochastic dynamics might arise for free particles on the quantum scale.

## SUPPLEMENTARY MATERIAL

See the [supplementary material](#) for movies of the pilot-wave field and MATLAB implementation of the numerical scheme governing the evolution of the pilot-wave system.

## ACKNOWLEDGMENTS

The authors gratefully acknowledge the NSF for financial support through Grant No. CMMI-1727565.

## APPENDIX A: NUMERICAL SCHEME

To derive the complex set of differential equations governing the evolution of the pilot-wave system (3), we first define the basis functions  $\Phi_n(\mathbf{x}) = J_n(r)e^{in\theta}$ , where  $(r, \theta)$  is the polar coordinate representation of  $\mathbf{x}$ . For use in the following derivation, we note that  $\Phi_n = (-1)^n \Phi_{-n}^*$  and

$$\nabla \Phi_n(\mathbf{x}) = \frac{1}{2} \Phi_{n-1}(\mathbf{x}) \begin{pmatrix} 1 \\ i \end{pmatrix} - \frac{1}{2} \Phi_{n+1}(\mathbf{x}) \begin{pmatrix} 1 \\ -i \end{pmatrix}. \quad (\text{A1})$$

To express the wave field in the particle frame of reference, we first write

$$h(\mathbf{x}, t) = \int_{-\infty}^t \Phi_0((\mathbf{x} - \mathbf{x}_p(t)) + (\mathbf{x}_p(t) - \mathbf{x}_p(s))) e^{-\mu(t-s)} ds.$$

Using Graf's addition theorem,<sup>47</sup>

$$\Phi_0(\mathbf{x} + \mathbf{y}) = \sum_{n=-\infty}^{\infty} \Phi_n(\mathbf{x}) \Phi_{-n}(\mathbf{y}),$$

we then express the wave field,  $h(\mathbf{x}, t)$ , as the basis decomposition<sup>13</sup>

$$h(\mathbf{x}, t) = \sum_{n=-\infty}^{\infty} a_n(t) \Phi_n(\mathbf{x} - \mathbf{x}_p(t)), \quad (\text{A2})$$

where the coefficients,  $a_n(t)$ , are defined as

$$a_n(t) = \int_{-\infty}^t \Phi_{-n}(\mathbf{x}_p(t) - \mathbf{x}_p(s)) e^{-\mu(t-s)} ds. \quad (\text{A3})$$

We note that the coefficients satisfy the reality condition  $a_n = (-1)^n a_{-n}^*$  for all integers  $n$ .

To express the coefficients in differential form, we differentiate (A3) with respect to  $t$ , yielding

$$\dot{a}_n(t) = \delta_{-n,0} - \mu a_n(t) + \dot{\mathbf{x}}_p(t) \cdot \int_{-\infty}^t \nabla \Phi_{-n}(\mathbf{x}_p(t) - \mathbf{x}_p(s)) e^{-\mu(t-s)} ds,$$

where  $\delta_{m,n}$  is the Kronecker delta. We evaluate the integral using Eq. (A1), from which we obtain the system of ordinary differential equations,

$$\dot{a}_n - \frac{1}{2} [\dot{z}_p a_{n+1} - \dot{z}_p^* a_{n-1}] + \mu a_n = \delta_{-n,0}, \quad \forall n \in \mathbb{Z}. \quad (\text{A4})$$

Here,  $z_p(t) = x_p(t) + iy_p(t)$  is the representation of the particle position,  $\mathbf{x}_p = (x_p, y_p)$ , in the complex plane. We then exploit the reality condition to restrict our attention to the coefficients with  $n \geq 0$ : the basis expansion (A2) for  $h(\mathbf{x}, t)$  is recast to give Eq. (4), and the system and the system of equations [Eqs. (A4)] may be reduced to the system (5a) and (5b). Finally, we use Eqs. (4) and (A1) to transform the particle evolution equation (3a) into a complex form, as given in Eq. (5c).

To account for the stiffness associated with the  $\kappa_0 \ll 1$  regime, we present a modification of the algebraic form of the particle trajectory equation (5c) in Subsection 1 of Appendix A. To initialize the pilot-wave system for steady rectilinear propulsion or circular orbits, we determine specific algebraic expressions for the wave field coefficients,  $a_n$ , as given in Subsections 2 and 3 of Appendix A, respectively. The magnitude of the coefficients in each of these

states determines a suitable truncation of the basis functions. Specifically, for a truncation parameter  $\delta > 0$ , we define the smallest integer  $N$  such that  $|a_n| < \delta$  for all  $n > N$  in a particular dynamical configuration. We then set  $a_n = 0$  for all  $n > N$ .

We note that the pilot-wave system (5) has no explicit dependence on the particle position,  $z_p(t)$ , reflecting the translational invariance of the system. Furthermore, the quadratic terms in (5a) and (5b) arise due to our centering of the wave field in the particle frame of reference and vanish when the particle is stationary. When the particle motion is confined to a line ( $y_p = 0$ ), all the terms in (5) are real and we recover the set of evolution equations derived by Durey *et al.*<sup>7</sup> We note that Perrard and Labousse<sup>48</sup> exploited a similar basis decomposition to evolve the pilot-wave system (3), but instead expressed the wave field,  $h(\mathbf{x}, t)$ , in a fixed frame of reference. As a consequence of imposing a fixed origin on the system, one cannot capture the translational invariance of the dynamics in a tractable manner. Finally, it is more efficient to evolve system (5) than recasting (3) as an integrodifferential equation for the particle position, as we need not integrate over the particle's prior trajectory in order to compute the wave force.<sup>10</sup> A more complete discussion of the numerical efficiency of different modeling approaches (including continuous systems and iterative maps) may be found in Turton *et al.*<sup>49</sup> and Bush and Oza.<sup>6</sup>

### 1. The overdamped limit

In the regime  $0 < \kappa_0 \ll 1$ , inertial effects arise on a fast time scale, resulting in a stiff dynamical system. To overcome the resultant stability issues arising when solving the pilot-wave system (5) numerically, we modify the algebraic form of the particle evolution equation, introducing an integrating factor to evolve the particle position analytically in the absence of a wave force.

We first define the time step  $\delta t$  and integration times  $t_l = l\delta t$  for all  $l \geq 0$ . To evolve the system from time  $t_l$  to time  $t_{l+1}$ , we follow the methodology of Milewski and Tabak.<sup>50</sup> Specifically, we multiply the particle evolution equation (5c) by the integrating factor  $e^{(t-t_l)/\kappa_0}$ , yielding

$$\frac{d}{dt} (\dot{z}_p e^{(t-t_l)/\kappa_0}) = -\frac{2}{\kappa_0} a_1^* e^{(t-t_l)/\kappa_0}.$$

We then introduce the modified velocity  $w_p(t) = \dot{z}_p(t) e^{(t-t_l)/\kappa_0}$ . Consequently, the particle evolution in the time interval  $t \in [t_l, t_{l+1}]$  may be expressed as the system

$$\dot{z}_p = w_p e^{-(t-t_l)/\kappa_0}, \quad (\text{A5a})$$

$$\dot{w}_p = -\frac{2}{\kappa_0} a_1^* e^{(t-t_l)/\kappa_0}, \quad (\text{A5b})$$

which couples with (5a) and (5b) to define the pilot-wave system. Notably, the particle velocity satisfies  $\dot{z}_p(t_l) = w_p(t_l)$  and  $\dot{z}_p(t_{l+1}) = w_p(t_{l+1}) e^{-\delta t/\kappa_0}$ . The pilot-wave system constituted by Eqs. (5a), (5b), and (A5) is then evolved numerically over the interval  $[t_l, t_{l+1}]$  using a fourth-order Runge-Kutta method.

### 2. Steady particle propulsion

We seek steady self-propelling states of the form  $z_p(t) = z_0 + u_0 t e^{i\phi}$ , where  $u_0$  is the steady propulsion speed [see Eq. (6)] and

$\phi$  is the direction of propulsion in the complex plane, so  $\mathbf{x}_p(t) = \mathbf{x}_0 + u_0 t(\cos \phi, \sin \phi)$ . Seeking constant solutions to the wave field coefficients [see Eqs. (5a) and (5b)] of the form  $a_n = D_n e^{-in\phi}$  gives rise to the difference equations,

$$-u_0 D_1 + \mu D_0 = 0,$$

$$\frac{u_0}{2} (D_{n-1} - D_{n+1}) + \mu D_n = 0, \quad \forall n \geq 1.$$

When coupled to the particle evolution equation (5c), this system of difference equations has the solution  $D_n = \rho \Theta^n$ , where  $\rho = (\mu^2 + u_0^2)^{-1/2}$  and  $\Theta = (\mu - \sqrt{\mu^2 + u_0^2})/u_0$ .<sup>7</sup> We then truncate the wave field coefficients,  $a_n$ , based on their magnitude,  $|a_n| = \rho |\Theta|^n$ .

### 3. Orbital solutions

We proceed to seek orbital solutions to (5), specifically,  $z_p(t) = z_0 + r_0 e^{i\omega_0 t}$  and  $a_n(t) = C_n e^{-in\omega_0 t}$ . From the integral representation of  $a_n(t)$  [see Eq. (A3)] with  $\mathbf{x}_p(t) = \mathbf{x}_0 + r_0(\cos \omega_0 t, \sin \omega_0 t)$ , we apply Graf's addition theorem<sup>47</sup> to obtain

$$C_n = i^n \int_0^\infty J_n \left( 2r_0 \sin \frac{\omega_0 s}{2} \right) e^{i\omega_0 s/2} e^{-\mu s} ds.$$

It is readily verified that  $a_n(t)$  satisfies the recurrence relations (5a) and (5b) for all  $n \geq 0$ . It remains, therefore, to determine the orbital radius,  $r_0$ , and angular frequency,  $\omega_0$ , using the equation of motion for the particle. The substitution of the orbital ansatz into the equation of particle motion [Eq. (5c)] determines that  $r_0$  and  $\omega_0$  satisfy the single complex equation,

$$-\kappa r_0 \omega_0^2 + ir_0 \omega_0 + 2C_1^* = 0,$$

or, equivalently,

$$i\kappa r_0 \omega_0^2 + r_0 \omega_0 = 2 \int_0^\infty J_1 \left( 2r_0 \sin \frac{\omega_0 s}{2} \right) e^{-i\omega_0 s/2} e^{-\mu s} ds.$$

By taking the real and imaginary parts of this equation, we recover the orbital equation (7).

To justify truncating the wave field coefficients,  $a_n(t)$ , when simulating orbital states, we note that

$$|a_n(t)| = |C_n| \leq \int_0^\infty \left| J_n \left( 2r_0 \sin \frac{\omega_0 s}{2} \right) \right| e^{-\mu s} ds \leq \frac{M_n}{\mu},$$

where

$$M_n = \max_{x \in [0, 2r_0]} |J_n(x)| \sim \frac{1}{\sqrt{2\pi n}} \left( \frac{er_0}{n} \right)^n \quad \text{as } n \rightarrow \infty.$$

The approximation<sup>51</sup> to the upper bound indicates that  $|a_n|$  exhibits exponential-like decay for large  $n$ , which we exploit to truncate the wave field coefficients for orbital motion.

### DATA AVAILABILITY

Data sharing is not applicable to this article as no new data were created or analyzed in this study.

### REFERENCES

- Y. Couder, S. Protière, E. Fort, and A. Boudaoud, "Walking and orbiting droplets," *Nature* **437**, 208 (2005).
- A. Eddi, E. Sultan, J. Moukhtar, E. Fort, M. Rossi, and Y. Couder, "Information stored in Faraday waves: The origin of a path memory," *J. Fluid Mech.* **674**, 433–463 (2011).
- E. Fort, A. Eddi, A. Boudaoud, J. Moukhtar, and Y. Couder, "Path-memory induced quantization of classical orbits," *Proc. Natl. Acad. Sci. U.S.A.* **107**, 17515–17520 (2010).
- S. Perrard, M. Labousse, M. Miskin, E. Fort, and Y. Couder, "Self-organization into quantized eigenstates of a classical wave-driven particle," *Nature Comm.* **5**, 3219 (2014).
- J. W. M. Bush, "Pilot-wave hydrodynamics," *Annu. Rev. Fluid Mech.* **47**, 269–292 (2015).
- J. W. M. Bush and A. U. Oza, "Hydrodynamic quantum analogs," *Rep. Prog. Phys.* **84**, 017001 (2021).
- M. Durey, S. E. Turton, and J. W. M. Bush, "Speed oscillations in classical pilot-wave dynamics," *Proc. Roy. Soc. A* **476**, 20190884 (2020).
- D. M. Harris, J. Moukhtar, E. Fort, Y. Couder, and J. W. M. Bush, "Wavelike statistics from pilot-wave dynamics in a circular corral," *Phys. Rev. E* **88**, 011001 (2013).
- D. M. Harris and J. W. M. Bush, "Droplets walking in a rotating frame: From quantized orbits to multimodal statistics," *J. Fluid Mech.* **739**, 444–464 (2014).
- A. U. Oza, Ø. Wind-Willassen, D. M. Harris, R. R. Rosales, and J. W. M. Bush, "Pilot-wave hydrodynamics in a rotating frame: Exotic orbits," *Phys. Fluids* **26**, 082101 (2014).
- P. J. Sáenz, T. Cristea-Platon, and J. W. M. Bush, "A hydrodynamic analog of Friedel oscillations," *Sci. Adv.* **6**, eaay9234 (2020).
- L. D. Tambasco, J. J. Pilgram, and J. W. M. Bush, "Bouncing droplet dynamics above the Faraday threshold," *Chaos* **28**, 096107 (2018).
- M. Hubert, S. Perrard, M. Labousse, N. Vandewalle, and Y. Couder, "Tunable bimodal explorations of space from memory-driven deterministic dynamics," *Phys. Rev. E* **100**, 032201 (2019).
- M. Durey, "Bifurcations and chaos in a Lorenz-like pilot-wave system," *Chaos* **30**, 103115 (2020).
- L. de Broglie, *Ondes et Mouvements* (Gautier Villars, 1926).
- L. de Broglie, *An Introduction to the Study of Wave Mechanics* (Methuen, 1930).
- A. U. Oza, R. R. Rosales, and J. W. M. Bush, "A trajectory equation for walking droplets: Hydrodynamic pilot-wave theory," *J. Fluid Mech.* **737**, 552–570 (2013).
- S. Protière, A. Boudaoud, and Y. Couder, "Particle-wave association on a fluid interface," *J. Fluid Mech.* **554**, 85–108 (2006).
- J. Moláček and J. W. M. Bush, "Drops walking on a vibrating bath: Towards a hydrodynamic pilot-wave theory," *J. Fluid Mech.* **727**, 612–647 (2013).
- P. A. Milewski, C. A. Galeano-Rios, A. Nachbin, and J. W. M. Bush, "Faraday pilot-wave dynamics: Modelling and computation," *J. Fluid Mech.* **778**, 361–388 (2015).
- M. Durey and P. A. Milewski, "Faraday wave-droplet dynamics: Discrete-time analysis," *J. Fluid Mech.* **821**, 296–329 (2017).
- Ø. Wind-Willassen, J. Moláček, D. M. Harris, and J. W. M. Bush, "Exotic states of bouncing and walking droplets," *Phys. Fluids* **25**, 082002 (2013).
- V. Bacot, S. Perrard, M. Labousse, Y. Couder, and E. Fort, "Multistable free states of an active particle from a coherent memory dynamics," *Phys. Rev. Lett.* **122**, 104303 (2019).
- A. U. Oza, D. M. Harris, R. R. Rosales, and J. W. M. Bush, "Pilot-wave dynamics in a rotating frame: On the emergence of orbital quantization," *J. Fluid Mech.* **744**, 404–429 (2014).
- M. Labousse, S. Perrard, Y. Couder, and E. Fort, "Self-attraction into spinning eigenstates of a mobile wave source by its emission back-reaction," *Phys. Rev. E* **94**, 042224 (2016).
- A. U. Oza, R. R. Rosales, and J. W. M. Bush, "Hydrodynamic spin states," *Chaos* **28**, 096106 (2018).
- T. Gilet, "Dynamics and statistics of wave-particle interactions in a confined geometry," *Phys. Rev. E* **90**, 052917 (2014).
- T. Gilet, "Quantum-like statistics of deterministic wave-particle interactions in a circular cavity," *Phys. Rev. E* **93**, 042202 (2016).

- <sup>29</sup>M. Durey, P. A. Milewski, and J. W. M. Bush, “Dynamics, emergent statistics, and the mean-pilot-wave potential of walking droplets,” *Chaos* **28**, 096108 (2018).
- <sup>30</sup>L. D. Tambasco and J. W. M. Bush, “Exploring orbital dynamics and trapping with a generalized pilot-wave framework,” *Chaos* **28**, 096115 (2018).
- <sup>31</sup>R. N. Valani and A. C. Slim, “Pilot-wave dynamics of two identical, in-phase bouncing droplets,” *Chaos* **28**, 096114 (2018).
- <sup>32</sup>A. Burinskii, “The Dirac–Kerr–Newman electron,” *Gravit. Cosmol.* **14**, 109–122 (2008).
- <sup>33</sup>E. Schrödinger, “About the force-free motion in relativistic quantum mechanics,” *Prus. Acad. Sci.* **31**, 418–428 (1930).
- <sup>34</sup>D. Hestenes, “The Zitterbewegung interpretation of quantum mechanics,” *Found. Phys.* **20**, 1213–1232 (1990).
- <sup>35</sup>E. Nelson, “Derivation of the Schrödinger equation from Newtonian mechanics,” *Phys. Rev.* **150**, 1079–1085 (1966).
- <sup>36</sup>H. C. Berg and D. A. Brown, “Chemotaxis in *Escherichia coli* analysed by three-dimensional tracking,” *Nature* **239**, 500–504 (1972).
- <sup>37</sup>H. C. Berg and E. M. Purcell, “Physics of chemoreception,” *Biophys. J.* **20**, 193–219 (1977).
- <sup>38</sup>Y. Pomeau and P. Manneville, “Intermittent transition to turbulence in dissipative dynamical systems,” *Commun. Math. Phys.* **74**, 189–197 (1980).
- <sup>39</sup>P. Richetti, F. Argoul, and A. Arneodo, “Type-II intermittency in a periodically driven nonlinear oscillator,” *Phys. Rev. A* **34**, 726–729 (1986).
- <sup>40</sup>A. P. Damiano, P.-T. Brun, D. M. Harris, C. A. Galeano-Rios, and J. W. M. Bush, “Surface topography measurements of the bouncing droplet experiment,” *Exp. Fluids* **57**, 1–7 (2016).
- <sup>41</sup>S. Perrard, M. Labousse, E. Fort, and Y. Couder, “Chaos driven by interfering memory,” *Phys. Rev. Lett.* **113**, 104101 (2014).
- <sup>42</sup>K. M. Kurianski, A. U. Oza, and J. W. M. Bush, “Simulations of pilot-wave dynamics in a simple harmonic potential,” *Phys. Rev. Fluids* **2**, 113602 (2017).
- <sup>43</sup>Y. Dagan and J. W. M. Bush, “Hydrodynamic quantum field theory: The free particle,” *Comptes Rendus. Mécanique* **348**, 555–571 (2020).
- <sup>44</sup>M. Durey and J. W. M. Bush, “Hydrodynamic quantum field theory: The onset of particle motion and the form of the pilot wave,” *Front. Phys.* **8**, 300 (2020).
- <sup>45</sup>A. Andersen, J. Madsen, C. Reichelt, S. Rosenlund Ahl, B. Lautrup, C. Ellegaard, M. T. Levinsen, and T. Bohr, “Double-slit experiment with single wave-driven particles and its relation to quantum mechanics,” *Phys. Rev. E* **92**, 013006 (2015).
- <sup>46</sup>A. Drezet, P. Jamet, D. Bertschy, A. Ralko, and C. Poulain, “Mechanical analog of quantum bradyons and tachyons,” *Phys. Rev. E* **102**, 052206 (2020).
- <sup>47</sup>M. Abramowitz and I. Stegun, *Handbook of Mathematical Functions* (Dover Publications, 1964), p. 363.
- <sup>48</sup>S. Perrard and M. Labousse, “Transition to chaos in wave memory dynamics in a harmonic well: Deterministic and noise-driven behavior,” *Chaos* **28**, 096109 (2018).
- <sup>49</sup>S. E. Turton, M. M. P. Couchman, and J. W. M. Bush, “A review of the theoretical modeling of walking droplets: Toward a generalized pilot-wave framework,” *Chaos* **28**, 096111 (2018).
- <sup>50</sup>P. A. Milewski and E. G. Tabak, “A pseudospectral procedure for the solution of nonlinear wave equations with examples from free-surface flows,” *SIAM J. Sci. Comput.* **21**, 1102–1114 (1999).
- <sup>51</sup>M. Abramowitz and I. Stegun, *Handbook of Mathematical Functions* (Dover Publications, 1964), p. 365.